ORIGINAL PAPER

Check for
updates

Fabrication and evaluation of structural, thermal, mechanical and optical behavior of epoxy–TEOS/MWCNTs composites for solar cell covering

Alaa M. Abd-Elnaiem[1] · **Seenaa I. Hussein**[2] · **Hasan S. Assaedi**[3] ·
A. M. Mebed[1,4]

Abstract

In the present study, hybrid organic–inorganic composites were fabricated from epoxy–TEOS (tetraethyl orthosilicate, $Si(OC_2H_5)_4$) with various ratios (0–10 wt%) of multiwall carbon nanotubes (MWCNTs) as reinforcing nanofillers by the sol–gel method. The effect of the MWCNTs ratios on the structural, optical and mechanical characteristics and the thermal conductivity of the epoxy–TEOS/MWC-NTs composites is investigated. The X-ray diffraction (XRD) analysis reveals that the pure epoxy-TEOS is amorphous, while epoxy–TEOS/MWCNTs composites are crystalline with an orthorhombic crystal structure that has an average crystallite size of 3.9 ± 0.15 nm. In addition, thermal stability and thermal conductivity were improved by adding TEOS and MWCNTs, whereas the exothermic peak temperature decreases compared with pure epoxy-TEOS. Similarly, the hardness Shore-D and tensile strength reach the optimum value at 4 wt% MWCNTs content. The significant improvement in the mechanical and thermal properties of the prepared composites could be attributed to the synergistic effect of MWCNTs and epoxy–TEOS which was emphasized by Fourier transform infrared (FTIR) spectroscopy. Moreover, epoxy-TEOS sample has high optical transmittance (T) within the visible region, but the composites samples are transparent at $\lambda < 800$ nm and have a lower value of T. The indirect optical band gap decreases from 3.59 to 2.91 eV with an increase in MWCNTs fractions from 0 to 10 wt%, respectively. However, the glass transition reflects the onset of decomposition temperatures was also considerably increased. The acquired outcomes such as a large increase in thermal conductivity

✉ Alaa M. Abd-Elnaiem
  abd-elnaiem@aun.edu.eg

1 Physics Department, Faculty of Science, Assiut University, Assiut 71516, Egypt

2 Department of Physics, College of Science, University of Baghdad, Baghdad, Iraq

3 Physics Department, Al Jumum University College, Umm Al-Qura University, P.O. Box 715, Mecca 21955, Saudi Arabia

4 Department of Physics, Faculty of Science, Jouf University, Sakaka 2014, Saudi Arabia

and tensile stress coupled with reduced T make the composites readily applicable for a variety of applications.

Graphic abstract
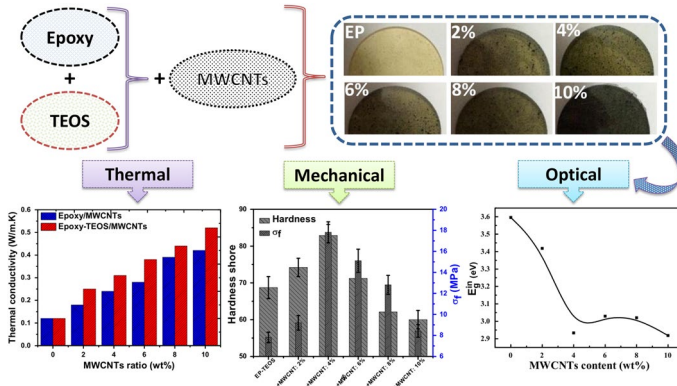
Keywords Epoxy · TEOS · MWCNTs · Thermal conductivity · Mechanical · Optical

Introduction

Conductive polymer composites are receiving attention because of the possibility of enhancing their optical and thermal conductivities as well as striking mechanical strength. Also, polymeric materials such as epoxy resin are of immense importance for their use as a matrix for advanced composites due to ease of processing and low cost. Such materials are gaining considerable attention because of their high specific strength, effective stiffness, chemical resistance and dimensional stability. However, the brittle nature and bad thermal and electrical conductivities of epoxy are considered a major drawback, especially when used for structural applications [1].

To overcome these undesirable properties of epoxy, several studies have been carried out to reinforce the epoxy with nanomaterials to form epoxy composites such as carbon nanotubes (CNTs), silicon carbide nanowires, magnesium oxide, titanium dioxide and calcium carbonate [2–8]. Among these fillers, CNTs are commonly used (compared to bulk carbon and other fillers) due to their desirable properties such as a high aspect ratio, and good mechanical, electrical and thermal properties, and other properties for arrays of applications [9, 10]. The physical properties of polymer/MWCNTs vary enormously depending on the synthesis and processing conditions [11]. MWCNTs have very low solubility in solvents and tend to remain as entangled agglomerates. It is proved that the key factor in optimizing the physical properties of polymer/MWCNTs is to achieve good dispersion and compatibility within the polymeric matrix. Many researchers have attempted to perform surface structure modification of CNTs through silanization reactions [12, 13], chemical grafting [14, 15] and β-hydroxyester surface functionalization [16]. However, such

methods cause morphological damage and severe degradation of CNTs [17, 18]. Epoxy-based composites can be used for many applications such as electrochemical sensing, and use in aircraft, capacitors actuators, etc. [19, 20].

The presence of CNTs in epoxy composites leads to excellent mechanical properties such ultra-high Young's modulus (~ 1 TPa) and high tensile strength (11–63 GPa) as well as exceptional thermal conductivity [21, 22]. Hadavand et al. examined the mechanical properties of MWCNTs/epoxy polysulfide nanocomposites [23] and their results showed better dispersion of modified MWCNTs than unmodified MWCNTs in a polymeric matrix which enhances the mechanical properties of the composites accordingly. Sapiai et al. studied the influence of functionalized MWCNTs on mechanical enhancement of kenaf fiber-reinforced polymer composites [24].

Similarly, the existence of MWCNTs in the polymer composite can enhance its thermal conductivity [25–28]. Standalone MWCNTs (SMWCNTs) and MWCNTs exhibit above-normal thermal conductivity over 3000 W/mK and 3500 W/mK, respectively [29]. However, the entangled network of CNTs sheets only shows the thermal conductivity of 20–30 W/mK at room temperature (RT) measured with the comparative methods [30, 31] and close to 80 W/mK with the bolometric technique [32]. Mi et al. studied the thermal conductivity of AlN–MWCNTs/cyanate ester composites with high flame retardancy and low dielectric loss [33]. The thermal conductivity, as a function of temperature, and glass transition temperature (T_g), as well as the curing behavior of some epoxy composites, was determined [34–36]. According to Gulotty et al. [37], functionalized MWCNTs can simultaneously enhance the electrical and thermal properties of the produced composites. Kareem stated the thermal and electrical properties of polyimide/polyaniline (PI/PANI) nanofiber composites prepared via in situ polymerization [38]. Gojny et al. [39] investigated the thermal and electrical conductivities of epoxy composites with various fillers such as single-walled, double-walled and MWCNTs as well as amino-functionalized CNTs from various producers. It was found that the addition or the existence of PANI nanofiber in the composite with the ratio ranging from 5 to 15 wt% resulted in a slight increase in the electrical activation energy of PI composites from 0.34 to 0.37 eV. Kargar et al. investigated the thermal properties of the epoxy composites with a high loading portion of graphene filler and some insulators such as boron nitride filler [40]. In addition, they devoted the study on the mechanism of the thermal percolation and thus facilitated the development of the next generation of efficient thermal interface materials for electronic applications. Moreover, Wang et al. investigated the effects of the fillers on the electrical and thermal conductivity of the cyanate ester resin [18].

Optical properties are widely used in a characterization method for investigating the electronic band structure of materials [41–44]. However, the relation between the filler types, concentrations and changes in the optical parameters of epoxy composites have not been studied in detail. Recently, Devangamath et al. [45] studied the optical parameters of epoxy–$CoSO_4.7H_2O$ polymer hybrid material. The filler loading is expected to significantly reflect the optical properties of the loaded polymer composites [41]. Therefore, it is important to study the optical properties of polymer composites for better understanding and also to extend their applications. Polymer films are especially ideal as specimens for optical reflectance (R) and transmittance

(*T*); they provide an accurate determination of the optical constants and absorption edge to be useful for interpreting the electronic structure of the materials. It was possible to determine the type of optical transition in band gap by optical absorption spectra [46]. It also suggests a possibility that the composite would be suitable for radiation shielding and solar cell covering [47].

According to the present research, electromagnetic (EM) shielding using polymer composites is mainly influenced by conductive material components such as MWC-NTs. Recently, additional conductive materials were used (besides the MWCNT components) to effectively improve the EM shielding of polymer composites such as polypyrrole (PPy) or Ag nanoparticles. For example, the synthesis of coaxial Ag@ PPy nanowires for effective EM wave absorption was carried out by Xie et al. [48]. In their study, the Ag–graphene/PPy showed remarkably increased current density, quicker response and better specific capacitance compared with graphene/PPy. Ternary nanocomposites of clay–Ag–PPy were prepared by chemical deposition or photoreduction, and some physical properties, e.g., thermal, optical, electrical and EM shielding properties, were investigated [49]. The formed clay–Ag–PPy nanocomposite revealed an enhancement in EM shielding effectiveness, thermal stability and electrical conductivity. A comparison of the EM shielding of the PPy–MWCNTs–Ag composites fabricated by chemical deposition and UV reduction was reported [50]. The comparison showed that the PPy–MWCNTs–Ag composite prepared by the UV reduction method has higher electrical conductivity as well as higher EM shielding effectiveness compared to a composite prepared by the chemical deposition method. In addition, the effect of Ag-doped graphene on electrochemical behaviors and specific capacitance of PPy-based nanocomposites was investigated by Kim et al. [51].

The thermal analysis methods such as differential thermal analysis (DTA) and differential scanning calorimetry (DSC) have been widely applied in the investigation of the characteristic temperatures occurring through heating of epoxy composites, *e.g.,* T_g, melting, crystallization and curing processes. The chemical composition of the composite greatly affects the value and nature of the T_g of the epoxy matrix composites [35, 36, 52–54]. Furthermore, the common deduced value of T_g for epoxy is about 154 °C enhanced to 177 °C by the incorporation of MWCNTs [36].

Generally, the epoxy is transparent with respect to visible light; however, it is brittle and has poor electrical and thermal properties. As mentioned above, the various morphologies of MWCNTs are commonly used as fillers among others to improve thermal, electrical, and mechanical properties. However, studies relating to the optical properties of such epoxy-based composites are extremely limited. In addition, doping epoxy with TEOS to form epoxy–TEOS/MWCNTs composites is proposed to increase the thermal stability of the composite. The addition of new material(s) to form a composite could affect the structural parameters, and accordingly, all physical and chemical properties will also be influenced. In the present study, the effect of the addition of MWCNTs and TEOS to epoxy forming epoxy–TEOS/MWCNTs composites on structural, mechanical, T_g, and thermal conductivity as well as optical properties was investigated and then compared with those of other similar composites. The results indicated that these properties could be effectively modulated by adjusting the fraction of MWCNTs as a filler and are influenced by the presence of TEOS. According to the present study, we observed that the prepared composite

could be suitable for shielding UV radiation, and for solar cell covering, as well as for use in heat spreaders and thermal pads.

Experimental details

Materials

Silica precursor—tetraethyl orthosilicate [$Si(OC_2H_5)_4$ or TEOS], was procured from Sigma-Aldrich (Germany), while ethanol (C_2H_5OH, 99.9% purity, 0.785 relative density) was obtained from Gainland Chemical Company (China). Deionized water was produced locally, and epoxy (105) was purchased from Don Construction Products (DCP). Hydrochloric acid (37% purity, 1.19 relative density) and MWCNTs (95% purity, 5–15 nm outside diameter) were obtained from US Nanomaterials Research, Inc. (USA).

Synthesis of silica and epoxy–TEOS/MWCNTs composites

Silica was synthesized by the sol–gel polymerization of TEOS. HCl was used as a hydrolysis and condensation catalyst. In the preparation, 5 ml of TEOS was diluted with 5 ml of ethanol; distilled water and HCl were then added to the mixture. The silica solution, molar ratio: $TEOS/C_2H_5OH/H_2O/HCl$ of 1:6:8:0.6, was vigorously stirred at 50 °C for 1 h. After refluxing for 2 h, MWCNTs of varying proportions were added to the silica mixture. Then, liquid hardener was slowly added to the epoxy resin at RT, and then, the mixture was vigorously stirred for 5 min. The ratio of hardener to epoxy was approximately 3:1. Composites of varying proportions were prepared by adding TEOS-coated MWCNTs to the epoxy where MWCNTs has different weight ratios (2, 4, 6, 8 and 10%). The mixtures were then stirred vigorously for 1 h in a glass tube to ensure homogeneity. The stirring process in the present study was carried out using a magnetic stirrer, while the temperature was controlled using a hot plate and was measured by a thermocouple. For more clarity, the procedures for the epoxy–TEOS/MWCNTs composite fabrication are presented schematically in Fig. 1.

Characterization of epoxy–TEOS/MWCNTs composites

The surface structures of samples of epoxy-TEOS and epoxy-TEOS/MWCNTs composites were examined using an optical microscope model Olympus BH 22. Thermal analysis was carried out via a differential scanning calorimeter (DSC, Shimadzu DSC-60) and a Shimadzu DTG-60H differential thermal analyzer. Thermal properties of polymer and polymer matrix composites were evaluated from T_g, the temperature at which polymer changes from ductile to brittle state due to a change in chain mobility. To do this, samples (3–10 mg) were heated from RT to 400 °C at a heating rate of 10 K min^{-1}. The measurements were taken in a dry nitrogen atmosphere. The phases, crystal size and texture for annealed samples were obtained

Fig. 1 A schematic illustration of the fabrication procedure of the epoxy–TEOS/MWCNTs composites
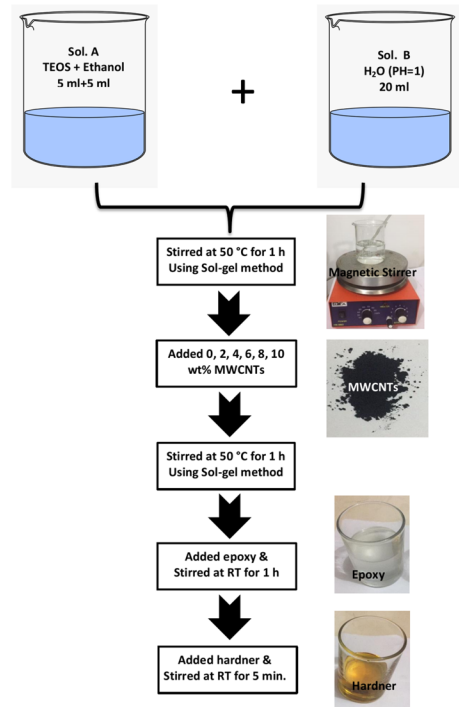
using a Phillips X-ray diffractometer. The spectral data were acquired within the range of $2\theta = 15°–90°$ at a scanning step and rate of 0.02° and 0.06°/s, respectively. The microstructures of some selected samples were obtained using SEM model JOEL-JSM-5400LV.

The most commonly used methods for determining the thermal conductivity are Searle's method and Lee's disc method, for good and bad conductors of heat, respectively. Therefore, we have used Lee's approach, where the experimental setup consists of four identical discs of 4 cm in diameter and ~6 mm thickness (optical image shown in Fig. 2a). The sample was placed in between discs A and B, while the power
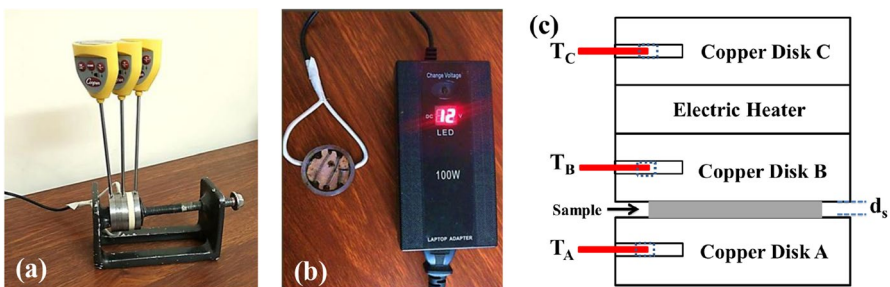

Fig. 2 **a** Setup of Lee's disc apparatus, **b** heater and DC power supply and **c** schematic drawing showing an arrangement of Lee's disc experiment [55, 56]

source/electric, shown in Fig. 2b, that supplies the heat (Duncan and Mark, 2001) was connected between the discs *B* and *C*. The arrangement of Lee's disc experiment is shown schematically in Fig. 2c. The epoxy composite samples were cut into circular disc shapes having the same diameters as other discs in Lee's method as shown in the optical images in Fig. 3. The DC power source had an operating voltage (*V*) of 12 V and current (*I*) of 0.5 A. The heat generated (*H*) from the power source (*H=IV*) was transferred to the discs in order of proximity to the heater. The disc's temperatures (T_A, T_B, and T_C) were measured with digital thermometers connected to the respective discs (Fig. 2a). The thermal conductivity coefficient (*K*) is calculated from Eqs. (1 and 2) [55, 56]:

$$K\frac{T_B - T_A}{d_s} = e\left[T_A + \frac{2}{r}\left(d_A + \frac{d_S}{4}\right)T_A + \frac{1}{2r}d_S T_B\right] \tag{1}$$

$$H = IV = \pi r^2 e\left(T_A + T_B\right) + 2\pi re\left[d_A T_A + \frac{d_S\left(T_A + T_B\right)}{2} + d_B T_B + d_C T_C\right] \tag{2}$$

where *e* is the amount of thermal energy passing through a unit area per second of the disc, *H* is the thermal energy passing through the heating coil per unit of time, d_S, d_A, d_B and d_C are the thicknesses of the samples and discs *A*, *B* and *C*, respectively, while *r* is the radius of the disc.

Hardness values of the samples were obtained using Shore-D hardness scales. The indirect tensile strength for the flattened geometry (σ_f) is obtained from Eq. (3) in accordance with the standard ASTM 6931 [57]:
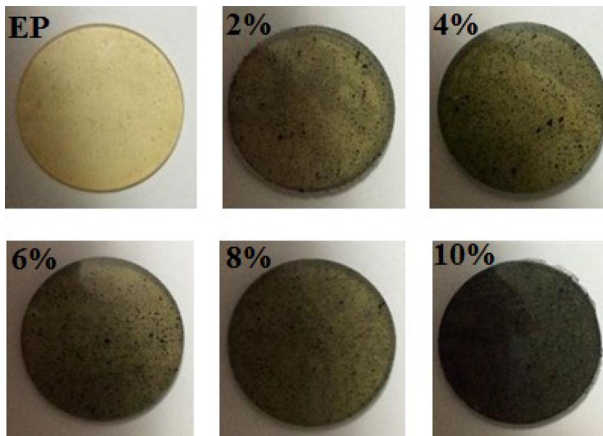
$$\sigma_f = \frac{F}{A_0} \tag{3}$$

Fig. 3 Samples of epoxy–TEOS/MWCNTs composites with different ratios of MWCNTs

where F is the applied force and A_0 is the original cross-sectional area. The hardness and the tensile stress values are estimated at least three times for the same condition, and then the average value is considered.

The values of $T(\lambda)$ and $R(\lambda)$ of the studied epoxy–TEOS/MWCNTs composites were recorded utilizing a double-beam spectrophotometer (Thermo-Scientific EV 300). The optical measurements were performed using unpolarized light at normal incidence at RT and at atmospheric pressure in the wavelength (λ) between 200 and 2500 nm. A specular reflection stage was attached to measure the reflectivity at normal incidence, using an Al mirror as a standard reference.

FTIR is a technique used to investigate the chemical bonds, especially in those hybrids in which silica is used as an inorganic phase. The FTIR measurements were recorded using a FTIR-8400S Shimadzu spectrometer with KBr discs ($400–4000$ cm^{-1}).

Results and discussion

Chemical properties

Figure 4, curve (a), shows the FTIR spectrum of the TEOS. From the FTIR spectra of the TEOS, some peaks are observed such as $3500–3750$ cm^{-1}, associated with H-bonded SiOH stretching vibrations and H-bonded water. One peak observed at 1650 cm^{-1} corresponds to the vibrations of molecular water. Two observed peaks at 1075 cm^{-1} and 795 cm^{-1} correspond to asymmetric and symmetric stretching vibrations of Si–O–Si and a bending Si–O–Si mode, respectively. An additional peak is observed at 952 cm^{-1}, which is related to the vibration of Si–OH bonding [58]. The absence of prominent C–H stretching bands over the $2800–3000$ cm^{-1} regions in the spectra suggests that the ethoxy groups were hydrolyzed during sol–gel synthesis, which is in good agreement with other work [59].

In the FTIR spectra of the epoxy resins in Ref [60], the bands observed at transmission peaks of 918 and 1675 cm^{-1} are ascribed to the vibrations of the epoxy ring and aldehyde groups, respectively. Meanwhile, broadband observed at 2925 cm^{-1} is attributed to the vibration of the aromatic protons.

Fig. 4 FTIR spectra of **a** TEOS, **b** epoxy–TEOS/2 wt% MWC-NTs and **c** epoxy–TEOS/10 wt% MWCNTs composites
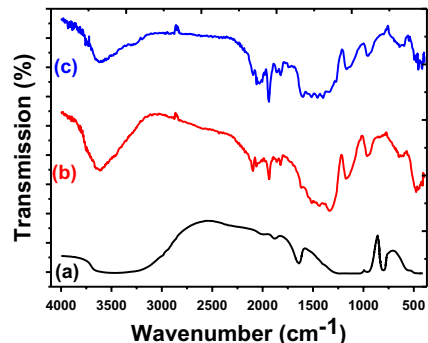
Figure 4, curves (b) and (c), shows the FTIR spectra of 2 wt% epoxy–TEOS/MWCNTs and 10 wt% epoxy–TEOS/MWCNTs composites, respectively. Both curves show the same peaks with some changes in the intensity, for example, a peak at 900 cm^{-1}, which is indicative of β-D-glucopyranosyl. Also, strong peaks can be observed in the range 1000–1200 cm^{-1} related to the C–O stretching of the superposition of C–O–C groups, which was inside and between the anhydroglucose ring and the C–O of the secondary hydroxyl and primary oxhydryl. The observed transmissions at 1116 cm^{-1} and 1037 cm^{-1} corresponded to the C–O stretching of the secondary hydroxyl and primary oxhydryl, respectively. Meanwhile, the observed peak at 2902 cm^{-1} was related to C–H bond stretching. In addition, a broad peak at 3422 cm^{-1} was ascribed to hydroxyl groups and hydrogen bonds. The spectrum of MWCNT–COOH demonstrated that the peak at 1089 cm^{-1} could be ascribed to carboxyl C–O bond stretching. The transmission peak at 1725 cm^{-1} was ascribed to carboxyl C=O bond stretching. The transmission peak at 3438 cm^{-1} was related to O–H bond stretching. New transmission from epoxy–TEOS/MWCNTs at 1735 cm^{-1}, 1070 cm^{-1} and 1157 cm^{-1} was ascribed to C=O and C–O–C bond stretching. The above transmission results reveal the formation of covalent bonds between epoxy–TEOS and MWCNTs.

Glass transition temperature

Distinguished T_g is considered as an important signature revealing the influence of the filler on the thermal property of the composites which the changes in the enthalpic, viscoelastic and dilatometric properties of the polymer matrix are expected.

Figure 5a presents the DSC curves for the epoxy–TEOS/MWCNTs composites. It is well defined that all samples show one principal T_g even for the neat resin. In addition, there is an endothermic peak (initial reaction temperature associated with a small fraction of resin homo-polymerization) observed within 60–90 °C. Filling with MWCNTs causes the small peak to decrease intensity and shifts with increased MWCNTs concentration. This might be attributed to the decomposition of organic groups and the elimination of water, CO and CO_2 trapped in the composite [61].

The glass transition peak appeared at 220 °C for the pristine sample decreased with filling by MWCNTs except for the filling with 4% where the transition temperature was raised up to 300 °C. As seen from Fig. 5b, the values of T_g change non-monotonically with composition due to the existence of different interphases between MWCNTs and the epoxy–TEOS polymer as a result of the presence of van der Waals force and the Coulomb attractions to form larger particles [62]. The weak force is largely responsible for increased T_g as MWCNTs content increased to 4%; beyond and above this, T_g decreases with MWCNTs. Moreover, the maximum uniform dispersion of MWCNTs (as shown in Fig. 8) and improved interfacial interaction between MWCNTs and epoxy matrix [63, 64] that attained around filler with 4 wt% caused the positive shift of Tg. In contrast, the MWCNTs agglomeration may cause the formation of free volume in the matrix and thus facilitate the motion of epoxy molecules, which leads to a drop in T_g [3, 65]. The distance between surface atoms of MWCNTs and polymer molecules, as well as larger interspace between the

Fig. 5 **a** DSC curves at the heating rate of 10 °C/min, for epoxy–TEOS/MWCNTs composites with different weights of MWCNTs, **b** the glass transition temperature (T_g) for all samples
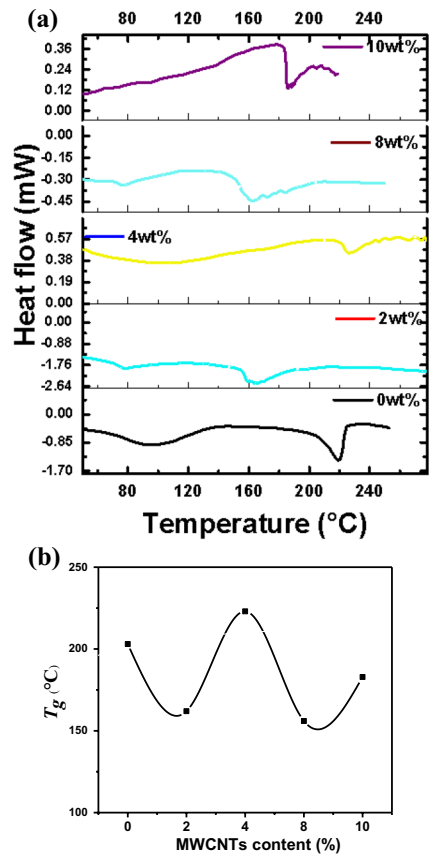
MWCNTs and the polymers, resulted in a decrease in T_g [66], and this might be the reason for a decrease in T_g at some MWCNTs contents. Moreover, the insignificant improvement for T_g except for the filling by 4% may be attributed to Kapitza resistance (the thermal resistance between the matrix and the filler) [67].

Figure 6a shows the thermogravimetric analysis (TGA) for epoxy-TEOS and epoxy-TEOS/MWCNTs composites in the temperature range RT–400 °C with a heating rate of 10 °C/min. It is generally observed, that there are three steps for weight loss for all samples. The first step starts from RT to about 100 °C, which is related to the evaporation of physically absorbed water and perhaps some residues of ethanol incorporated through the drying process. The second step of weight loss falls between 100 and 300 °C, attributed to the removal of oxygen-containing groups on the surface. The third weight loss step is between 300 and 400 °C, attributed to the combustion of residual organic. The values of weight loss through selected ranges of temperatures (RT–220 °C; 220–400 °C), as well as the total weight loss during the heating from RT to 400 °C, are listed in Table 1. As observed from the table, all the samples reveal lower weight loss than the pure epoxy except samples containing 6 wt% MWCNTs. The observation could be attributed to the

Fig. 6 a The TGA curves with a heating rate of 10 °C/min from RT to 400 °C under N_2 flow for epoxy–TEOS/MWCNTs composites and **b** the derivative of the TGA curve
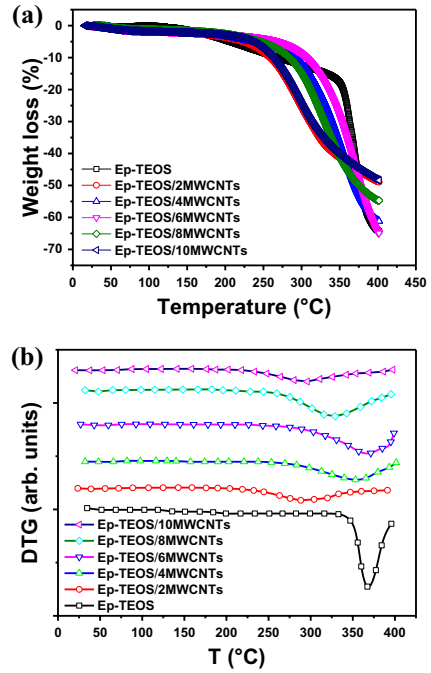

Table 1 Weight loss (m_{loss}) and decomposition temperature ($T_{deco.}$) of epoxy–TEOS/MWCNTs composites through thermal heating at various temperatures obtained from the TGA curves

Sample	Epoxy	Epoxy–TEOS/MWCNTs				
		2 wt%	4 wt%	6 wt%	8 wt%	10 wt%
m_{loss} between RT–220 °C	6.12	4.77	4.31	3.01	3.52	3.67
m_{loss} between 220–400 °C	58.16	43.95	56.67	61.44	51.09	44.53
Total m_{loss} RT–400 °C	64.28	48.72	60.98	64.45	54.61	48.2
$T_{deco.}$ (°C)	367.3	291.68	354.22	369.22	328.83	294.78

increase in thermal conductivity of epoxy polymer as a result of addition of MWC-NTs. The presence of MWCNTs enhances the heat diffusion and, therefore, leads to faster degradation of the epoxy composites. Moreover, the enhanced thermal stability of epoxy–TEOS/MWCNTs composites compared to pure epoxy could be attributed to the increase in the degree of cross-linkage as well as in the crystallinity of matrix material. In addition, the decomposition temperature for the epoxy and its composites is listed in Table 1 and determined from the derivative of the TGA curve as shown in Fig. 6b. All the estimated temperatures for the decomposition process are lower for epoxy composites as compared to pure epoxy. All samples show a single decomposition peak between 300 and 376 °C, which is related to the decomposition of urethane linkages and soft segments of thermoplastic polyurethane [68].

During the melting of a polymer, there is a rearrangement of the molecules in the transformation from ordered to disordered molecular states. Molecular chemistry and structure influence the ability of the polymer chain molecules to make these rearrangements and, therefore, will also affect the transition temperatures. When the ratio of MWCNTs in the mixture with respect to the polymer and MWCNTs consists of the network between the polymer and MWCNTs, they overlap between the chains to limit water molecules leading to the higher thermal stability of the final output.

The above results reveal that the thermal stability of epoxy composites containing TEOS and MWCNTs is enhanced compared to pristine epoxy up to a definite limit of filling.

X-ray analysis

The effect of incorporation of MWCNTs on the crystal structure of the epoxy–TEOS/MWCNTs composite was analyzed by XRD, as presented in Fig. 7. The spectra reveal a broad peak at 18° for pristine composite, which reveals the amorphous nature of epoxy–TEOS, while samples loaded with MWCNTs show varying degrees of crystallinity. The epoxy–TEOS/MWCNTs composites show a sharp diffraction peak associated with MWCNTs with almost no shift at $2\theta = 25.6°$ and extra two low-intensity peaks at 53.1° and 72.15° assigned to the reflectance from planes (110), (220) and (312), respectively. The samples have orthorhombic crystal structure based on ICDD card no 01089849 [69]. This suggests that the addition of MWCNTs disrupts the existing structure of epoxy–TEOS. The average crystallized size, obtained from Scherrer's equation, is 3.9 ± 0.15 nm. The estimated d-spacing values are 3.56, 1.92 and 1.6 Å for planes (110), (220) and (312), respectively. Similarly, the ASTM d-spacing values are 3.45, 1.72 and 1.303 Å.

Fig. 7 XRD chart for epoxy–TEOS and different epoxy–TEOS/MWCNTs composites
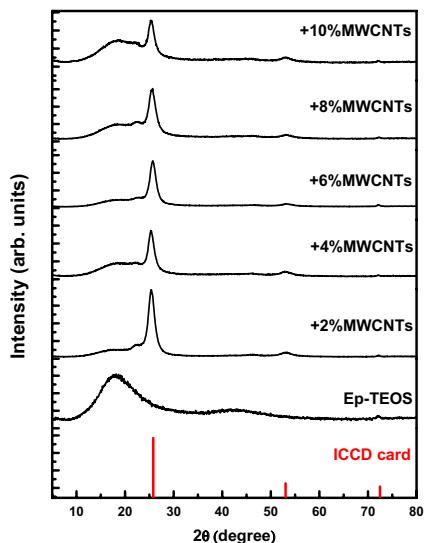
Morphology

Optical micrographs show that the texture distribution of the MWCNTs within the epoxy–TEOS matrix is influenced by the different surface functionalization. The optical images, as shown in Fig. 8, show the MWCNTs embedded in the epoxy–TEOS matrix that appears as black particles. As the MWCNTs content increases, both the density and size of this aggregate particle increase. It is evident from the micrographs that the fillers are well dispersed in the whole medium of the polymer for low loadings up to 4 wt% and, however, re-agglomeration of MWCNTs at high loadings (> 4 wt%) in epoxy–TEOS is in good agreement with other work [70]. MWCNTs are known to agglomerate and entangle easily due to their size and high aspect ratio. The average aggregate dimension was evaluated within the range 4–8 μm, confirming that adding TEOS alongside the epoxy helps MWCNTs aggregate less.

In order to check the morphology of the synthesized samples or MWCNTs dispersion in the epoxy-TEOS matrix, samples with various concentrations of MWCNTs were investigated by means of the SEM. Figure 9 shows the SEM images of epoxy–TEOS with 0 wt%, 4 wt%, 8 wt% and 10 wt% MWCNTs. In a homogeneous morphology, the MWCNTs are uniformly distributed in a close net through the epoxy matrix for filling with 4 wt%. The figure shows that the TEOS coated with MWCNTs has a tendency to become rougher with increase in the contents of MWCNTs. For example, Fig. 9d demonstrates a rough structure in the case of epoxy–TEOS with 10 wt% MWCNTs which may indicate the structure of agglomerated MWCNTs particles. The observed bright agglomeration in the SEM images could be due to the TEOS particle in the matrix.
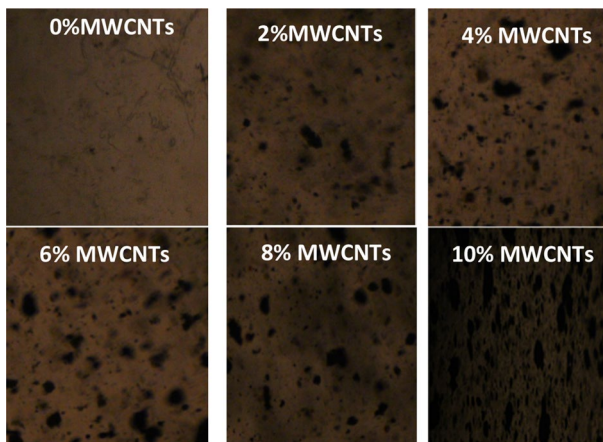

Fig. 8 Optical images of epoxy–TEOS/MWCNTs composites (magnification 500X)
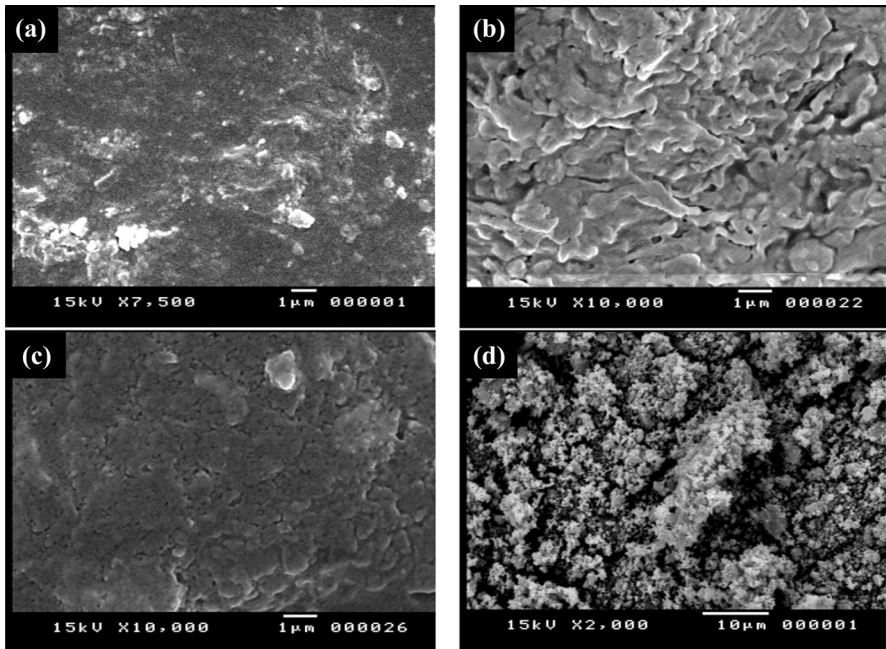
Fig. 9 SEM images showing the top view of **a** epoxy–TEOS, **b** epoxy–TEOS/4 wt% MWCNTs, **c** epoxy–TEOS/8 wt% MWCNTs, **d** epoxy–TEOS/10 wt% MWCNTs

Thermal conductivity

Figure 10 shows the change in thermal conductivity for epoxy–TEOS/MWCNTs composites versus the MWCNTs fraction. It is clear that thermal conductivity is improved by the addition of the MWCNTs filler. Thermal conductivity is doubled by adding 2 wt% of MWCNTs to the composite. As the filler increased to 10 wt%, the thermal conductivity increased by 333% or about 4.3-fold. This observation agrees with the findings reported by Kareem [38] as well as the 2.6-fold increase observed by Ramirez et al. for nanostructured ferrimagnetic iron oxide composites [71]. For

Fig. 10 Thermal conductivity of epoxy/MWCNTs and epoxy–TEOS/MWCNTs composites as a function of MWCNTs content
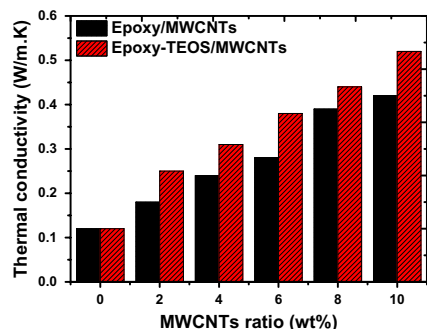
this study, the value of K increases linearly with a fraction of the MWCNTs fillers, x, according to Eq. 4.

$$K = 0.0377x + 0.148. \tag{4}$$

A plausible explanation for the large observed increase in the thermal conductivity is attributed to the high intrinsic thermal conductivity of MWCNTs as well as good contact between the filler and the matrix [29]. This becomes more significant as the filler loading and dispersion, as well as the thermal resistance of the interface between the fillers and matrix, improved. Saadah et al. also reported that graphene fillers are responsible for the improved thermal conductivity of thermal interface materials when used for solar cell applications [72]. It is, however, possible for the TEOS to further improve the thermal conductivity of the composite by de-bundling MWCNTs to promote more uniform dispersion and adhesion to the matrix through effective interfacial bonding [10, 27, 54].

Mechanical properties

The Shore-D hardness values and indirect tensile strength of epoxy composites were evaluated and are presented in Fig. 11a and b. As the MWCNTs content increased up to 10 wt%, both Shore-D hardness and tensile strength of epoxy composites increase at first as the MWCNTs content reaches 4 wt% compared to the pristine sample and then begin to decline. Moreover, the maximum uniform dispersion of MWCNTs and strong interfacial interaction between MWCNTs and epoxy-TEOS matrix is attained around filler with 4 wt% to further facilitate mechanical approval. These measurements agree well with the morphological structure obtained in Fig. 7.

It is evident that the hardness initially increased from 68.7 for the pure epoxy–TEOS composite to 82.9 for epoxy modified with 4 wt% MWCNTs. Further increase in the MWCNTs beyond 6 wt% leads to a reduction in the hardness value below that of the pure epoxy–TEOS. The hardness that initially increased indicates reduced ductility, and consequently, the composites become more brittle as more MWCNTs are added. Similarly, the tensile strength does not increase monotonically with MWCNTs loading. From 7.81 MPa for pure epoxy–TEOS composite, the

Fig. 11 Hardness Shore-D and the tensile strength (σ_f) for epoxy–TEOS/MWCNTs composites
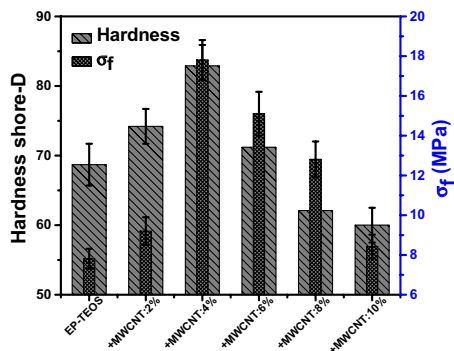
strength increased by 230% at 4 wt% MWCNTs loading. The substantial increase in mechanical performance can be attributed to better covalent bonding between the nanofillers and epoxy–TEOS resin. However, at higher fraction hardness and tensile stress decreased due to possible MWCNTs agglomeration, viscosity buildup, incomplete MWCNTs wetting by polymer and their poor dispersion within the epoxy matrix leading to brittle behavior [22]. Therefore, for optimum hardness and tensile strength, the fraction of MWCNTs must be kept at about 5 wt%. The improvement in the mechanical properties of the composites could be attributed to the synergistic effect of MWCNTs with epoxy–TEOS. It is believed that the MWCNTs provide mechanical interlocking with the matrix interface and thus improve the interfacial interaction as shown in the SEM image (Fig. 7). The MWCNTs in epoxy–TEOS provide a good contribution to the improvement in the mechanical properties of the composites, while MWCNTs in epoxy only show a negligible improvement in the mechanical properties in accordance with the work of Ci and Bai [73].

Optical properties

Among many applications of the epoxy resins, their thin films were used as a base solar cell plate and paints for different porous materials. Therefore, elaborating the optical properties of the epoxy composite for EM spectrum to cover the UV, visible and IR regions for λ from zero to 2500 nm is needed. The absorption should occur if there is a resonance between the energy of the EM wave and the electronic states [74]. Generally, the higher energy part of the spectrum gives information about the electronic states in the normal material, whereas the lower energy part gives information about the atomic vibrations [47].

Various optical parameters could be obtained, and a particular emphasis was placed on T, absorption coefficient (α), R and E_g for these discs with respect to determination and analysis of the parameters. The influence of MWCNTs on the T versus λ of the composites is shown in Fig. 12. It can be seen that for all filler levels, the composite films show high transparency in the visible region of the EM spectrum ($\lambda = 380–850$ nm), while it is almost null for the UV region.

Furthermore, T, which decreased with MWCNTs content, shows a high degree of oscillation indicating samples of large size. The T edge shifts toward higher λ as MWCNTs increased leading to the lower optical band gap. The pristine sample

Fig. 12 Transmittance (T) for discs of epoxy–TEOS/MWCNTs composites with different weights of MWCNTs
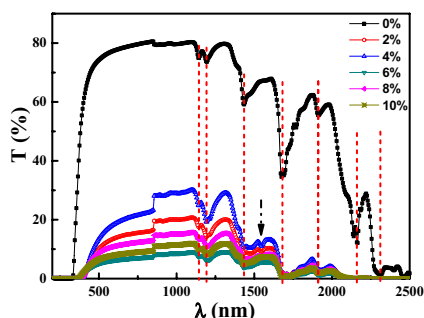
shows peaks at 1200 with shoulder, 1440, 1670, 1920, 2150 and 2300 nm. However, upon blending the MWCNTs with epoxy–TEOS, the IR spectra of composites show lower intensity peak with no shift in their positions at 1200, 1440, 1670 and 1920 nm, while the 2150 and 2300 nm disappear. This indicates that the presence of such IR bands in the spectra of composites only reflects the superposition of MWCNTs and epoxy bands and no obvious changes occur in the graphitized structure of MWCNTs after their being introduced into the composite [75], which means that there are certain interactions between them. The characteristic peak of the MWCNTs at 1550 nm strongly appears for 4 wt% MWCNTs, and also for 6 wt% and 8 wt%. The low intensity observed for MWCNTs indicates that the present MWCNTs have a low degree of graphitization.

In general, the behavior of the T of pristine sample is higher than the composites for the entire MWCNTs ratio. However, the absolute value of R slightly decreases with MWCNTs (Fig. 13) for the higher λ. The inserted graph presented in Fig. 13 shows the magnified spectra in the UV and IR range. In the R plots shown in Fig. 13, an obvious peak is seen for all samples in the UV, not in the visible region. The trend of the T & R at the IR range of higher λ may be attributed to the interaction of EM waves with the free carrier absorption [76, 77]. However, as shown in the inset graph in Fig. 13 two peaks are generated at 250 and 310 nm, indicating that there is a significant electronic interaction in the ground state between MWCNTs and epoxy. Therefore, the addition of MWCNTs up to 8 wt% to epoxy–TEOS will enhance their UV reflectance. The null T and the absorption peak lying in the UV region, indicates the absorption of the high-energy photons in the UV region, making the composite suitable for UV shielding and also can be used as a cover to protects the solar cell from UV damage. In the visible region, no such effect is observed. It can also be seen that the increase in MWCNTs weight fraction in epoxy–TEOS composite causes a slight blue shift within 3–5 nm in the peak maximum at 310 nm, and this may signify that the effective conjugation length of epoxy–TEOS becomes extended in the composite. It was noticed that the position and intensity of the peaks depend on the composition content of the sample. As the λ in the UV spectral regions increased, the T increases sharply, while the R decreases exponentially as shown in Figs. 12 and 13.

From the experimentally measured values of T and R, the absorption coefficient, α, is calculated using Eq. (5) [78] in which d is the sample thickness.

Fig. 13 Reflectance (R) for discs of epoxy–TEOS/MWCNTs composites with different weights of MWCNTs
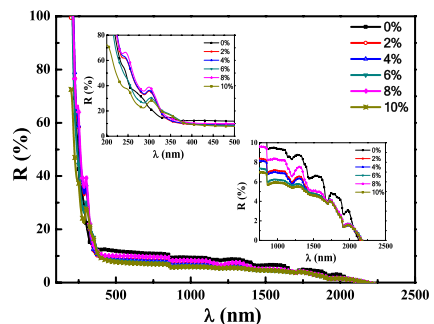
$$\alpha = \frac{1}{d} \ln \left[\frac{(1-R)^2 + [(1-R)^4 + 4T^2R^2]^{1/2}}{2T} \right]. \qquad (5)$$

In optical materials, the absorption coefficient, α, can be classified into three regions: (i) high absorption region ($\alpha > 10^4$ cm^{-1}) which is attributed to the transition from band to band that determines the E_g, (ii) edge region which is due to the structure randomness and (iii) a weak absorption tail region which is due to defects or impurities [79]. Usually, new absorption peaks are expected if there is a ground-state electronic interaction between the components in a blend composite matrix [80]. For the pristine MWCNTs [41] and also epoxy, there are no absorption or R peaks that are observed in the UV range. These regions were the weak absorption level, which originates from the experimental edge region, and show strong relation to the structural randomness of the system, and the high absorption region, which determines the E_g.

Nowadays, it is known that the band structures of materials influence the electronic properties of materials, and hence band gap studies on hybrid materials are important. For amorphous materials, Mott–Davis relation correlates the absorption coefficient to photon energy. In other words, the value of α depends on a frequency (v). According to Eq. (6) [81, 82]:

$$(\alpha h v) = B(h v - E_g)^m \qquad (6)$$

where h is the Planck constant, B is the disorder parameter having a constant between 10^5 and 10^6 cm^{-1} eV^{-1} [83] and m is the number which recognizes the transition process having a value of 1/2 for direct allowed transition, 2 for indirect allowed transition and 3/2 and 1/3 for direct forbidden and indirect forbidden transitions, respectively [84]. The dependency of $(\alpha h v)^{1/m}$ on photon energy is plotted for different values of m for epoxy-TEOS composites with different contents of MWCNTs. The result showed that the major type of transition has an indirect allowed transition, indicating the interaction of EM waves with the electrons in the valance bands. Figure 14 shows the dependence of $(\alpha h v)^{1/2}$ on $(h v)$ for all samples with an emphasis on the absorption region. Changes in the band gap of hybrid composites are seen due to the structural changes caused by the incorporation of MWCNTs

Fig. 14 $(\alpha h v)^{1/2}$ versus $h v$ for epoxy–TEOS/MWCNTs composites with different weights of MWCNTs
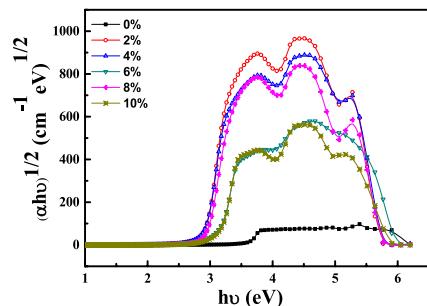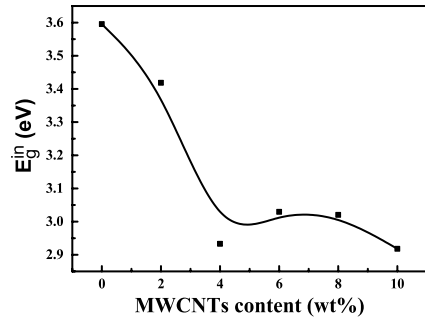
Fig. 15 Indirect optical band gap (E_g^{in}) for epoxy–TEOS/MWCNTs composites with different weights of MWCNTs

in the epoxy composite [45]. It is interesting to see an appreciable change in the band gap with different contents of MWCNTs.

The E_g^{in} (Fig. 15) is obtained by extrapolating the linear portions of the plots to intersect the energy axis in Fig. 14. On investigating the values of energy band gaps, it is seen that the variation of the band gap decreasing to a minimum value at 2.94 eV, corresponding to epoxy–TEOS with 4 wt% MWCNTs, and slightly increases again with increasing the MWCNTs content. This may be attributed to the increase in the crystallinity of the samples [85, 86] or to the intimate mixing of filler particles within the polymer matrix, leading to altered energy states between valence and conduction bands of the host matrix. It is concluded that at a particular filler level of 4 wt%, the composite could show better optical with lower energy gap and mechanical properties with a homogeneous structure. These optical measurements and analyses confirm the successful influence of the filler in the matrix.

Conclusion

We started with synthesized hybrid epoxy and TEOS and then modified it with MWCNTs. The optimized loading was found to be 4 wt% MWCNTs, where the mechanical, optical, and thermal properties of epoxy composites reached the optimum values. With a filling of 4 wt% MWCNTs, the tensile strength of epoxy composites increased by 42.0% and 20.3%, respectively, and the T_g and thermal decomposition temperatures were significantly increased by 80 °C with reference to the pristine sample. This is attributed to the effective dispersion of MWCNTs and the existence of the TEOS, leading to the formation of strong interfacial bonding. The optical properties of these composites were studied by analyzing the experimental T and R data. There are two peaks generated for the composite, irrespective of the pristine sample in the UV region at 250 and 310 nm indicating the significant electronic interaction in the ground state between MWCNTs and epoxy. The optical results showed that the transition has an indirect allowed type with different composites of epoxy–TEOS/MWCNTs. These values of optical band gap were seen to be decreasing with increased MWCNTs contents to attain its minimum value for filling at 5 wt%, which is attributed to the increase in the crystallinity of the samples.

These results can indicate the possibility of utilizing the obtained composites for applications in which low absorbance is demanded in the region that falls near the UV region.

References

1. Yemam D, Kim B-J, Moon J-Y, Yi C (2017) Mechanical properties of epoxy resin mortar with sand washing waste as filler. Materials 10(3):246
2. Hussein SI, Abd Elnaiem AM, Asafa TB, Jaafar HI (2018) Effect of incorporation of conductive fillers on mechanical properties and thermal conductivity of epoxy resin composite. Appl Phys A 124(7):475
3. Zeng S, Shen M, Yang L, Xue YC, Lu F, Chen S (2018) Self-assembled montmorillonite–carbon nanotube for epoxy composites with superior mechanical and thermal properties. Compos Sci Technol 162(7):131–139
4. Burger N, Laachachia A, Ferriolb M, Lutzc M, Toniazzoa V, Ruch D (2016) Review of thermal conductivity in composites: mechanisms, parameters and theory. Prog Polym Sci 61:1–28
5. Shen D, Zhan Z, Liu Z, Cao Y, Zhou L, Liu Y, Dai W (2017) Enhanced thermal conductivity of epoxy composites filled with silicon carbide nanowires. Sci Rep 7(1):2606
6. Fei-Peng D, Tang H, Huang D-Y (2013) Thermal conductivity of epoxy resin reinforced with magnesium oxide coated multiwalled carbon nanotubes. Int J Polym Sci 2013:Article ID 541823
7. Congliang H, Zhen W, Huang Z, Luo D (2018) Thermal and electrical conductivities of epoxy resin-based composites incorporated with carbon nanotubes and TiO_2 for a thermoelectric application. Appl Phys A 24(1):38
8. Backesa EH, Senea TS, Passadorb FR, Pessan LA (2018) Electrical, thermal and mechanical properties of epoxy/CNT/calcium carbonate nanocomposites. Mater Res 21(1):e20170801
9. Dresselhaus MS, Dresselhaus G, Eklund PC, Rao AM (2000) Carbon nanotubes. In: Andreoni W (ed) The physics of fullerene-based and fullerene-related materials. Springer, Netherlands, pp 331–379
10. Campbell FC (2010) Structural composite materials. ASM international, Cleveland
11. Ahmadi Z (2019) Epoxy in nanotechnology: a short review. Prog Org Coat 132:445–448
12. Lee JH, Rhee KY, Park SJ (2011) Effect of silane modification and temperature on tensile and fractural behaviours of carbon nanotube/epoxy nanocomposites. J Nanosci Nanotechnol 11:275–80
13. Avilés F, Cauich-Rodríguez JV, Rodríguez-González JA, May-Pat A (2011) Oxidation and silanization of MWCNTs for MWCNT/vinyl ester composites. Express Polym Lett 9:766–776
14. Wang S, Liang Z, Liu T, Wang B, Zhang C (2006) Effective aminofunctionalization of carbon nanotubes for reinforcing epoxy polymer composites. Nanotechnology 17(6):1551–1557
15. Shen JF, Huang W, Wu L, Hu Y, Ye M (2007) The reinforcement role of different amino-functionalized multi-walled carbon nanotubes in epoxy nanocomposites. Compos Sci Technol 67(15–16):3041–3150
16. Chen W, Auad ML, Williams RJ, Nutt SR (2006) Improving the dispersion and flexural strength of multiwalled carbon nanotubes–stiff epoxy composites through β-hydroxyester surface functionalization coupled with the anionic homopolymerization of the epoxy matrix. Eur Polym J 42:2765–72
17. Meng H, Sui G, Fang P, Yang R (2008) Effects of acid-and diamine-modified MWNTs on the mechanical properties and crystallization behavior of polyamide 6. Polymer 49(2):610–620
18. Wang X, Zhao Y, Jin J, Song M (2017) A comparative study on the effect of carbon fillers on electrical and thermal conductivity of a cyanate ester resin. Polym Test 60:293–298
19. Pumera M, Merkoçi A, Alegret S (2006) Carbon nanotube-epoxy composites for electrochemical sensing. Sens Actuators B Chem 113:617–622
20. Yun Y-H, Shanov V, Schulz MJ, Narasimhadevara S, Subramaniam S, Hurd D, Boerio FJ (2005) Development of novel single-wall carbon nanotube–epoxy composite ply actuators. SMART Mater Struct 14:1526–1532
21. Sumio I (1991) Helical microtubules of graphitic carbon. Nature 354:56–58
22. Arash B, Wang Q, Varadan VK (2014) Mechanical properties of carbon nanotube/polymer composites. Sci Rep (Nature Publisher Group) 4:6479

23. Hadavand BS, Javid KM, Gharagozlou M (2013) Mechanical properties of multi-walled carbon nanotube/epoxy polysulfide nanocomposite. Mater Des 50:62–67

24. Sapiai N, Jumahat A, Mahmud J (2018) Mechanical properties of functionalised CNT filled kenaf reinforced epoxy composites. Mater Res Express 5(4):045034

25. Jinho H, Jeongwoo L, Chang H, Sang S (2010) Improvement of thermal conductivity of poly (dimethyl siloxane) using silica-coated multi-walled carbon nanotube. J Therm Anal Calorim 101(1):297–302

26. Jiaxi G, Saha P, Liang J, Saha M, Grady BP (2013) Multi-walled carbon nanotubes coated by multi-layer silica for improving thermal conductivity of polymer composites. J Therm Anal Calorim 113(2):467–474

27. Z. Jinchao, F. Du, W. Cu, P. Zhu, X. Zhou and X. Xie., Effect of silica coating thickness on the thermal conductivity of polyurethane/SiO2 coated multiwalled carbon nanotube composites, Composites Part A: Applied Science and Manufing, vol. 58, pp. 1–6, 2014.

28. An L, Zhang C, Zhang Y-F (2017) Thermal conductivity of graphene-polymer composites: Mechanisms, properties, and applications. Polymers 9(9):437

29. Kim P, Shi L, Majumdar A, McEuen P (2001) Thermal transport measurements of individual multi-walled nanotubes. Phys Rev Lett 87:215502

30. Gonnet P, Liang Z, Choi E, Kadambala R, Zhang C, Brooks J et al (2006) Thermal conductivity of magnetically aligned carbon nanotube buckypapers and nanocomposites. Curr Appl Phys 6:119–122

31. Hone J, Llaguno M, Nemes N, Johnson A, Fischer J, Walters D et al (2000) Electrical and thermal transport properties of magnetically aligned single wall carbon nanotube films. Appl Phys Lett 77:666–668

32. Itkis M, Borondics F, Yu A, Haddon R (2007) Thermal conductivity measurements of semitransparent single-walled carbon nanotube films by a bolometric technique. Nano Lett 7:900–904

33. Ya-nan M, Liang G, Gu A, Zhao F, Yuan L (2013) Thermally conductive aluminum nitride–multi-walled carbon nanotube/cyanate ester composites with high flame retardancy and low dielectric loss. Ind Eng Chem Res 52(9):3342–3353

34. Ali SS, Al-Muaikel NS (2010) Thermal properties of epoxy (DGEBA)/phenolic resin (NOVOLAC) blends. Arab J Sci Eng 35(1B):7–14

35. Ao L, Li W, Ling Y, Gan W, Brady MA, Wang C (2016) Effects of silica-coated carbon nanotubes on the curing behavior and properties of epoxy composites. RSC Adv 6(28):23318–23326

36. Jiang C, Zhang J, Lin S, Ju S, Jiang D (2015) Effects of free organic groups in carbon nanotubes on glass transition temperature of epoxy matrix composites. Compos Sci Technol 118:269–275

37. Gulotty R, Castellino M, Jagdale P, Tagliaferro A, Balandin AA (2013) Effects of functionalization on thermal properties of single-wall and multi-wall carbon nanotube–polymer nanocomposites. ACS Nano 7(6):5114–5121

38. Kareem AA (2018) Thermal and electrical properties of polyimide/PANI nanofiber composites prepared via in situ polymerization. Mater Sci Poland 36(2):283–287

39. Gojny FH, Wichmann MH, Fiedler B, Kinloch IA, Bauhofer W, Windle AH, Schulte K (2006) Evaluation and identification of electrical and thermal conduction mechanisms in carbon nanotube/epoxy composites. Polymer 47:2036–2045

40. Kargar F, Barani Z, Lewis JS, Debnath B, Salgado R, Aytan E, Lake R, Balandin AA (2018) Thermal percolation threshold and thermal properties of composites with high loading of graphene and boron nitride fillers. ACS Appl Mater Interfaces 10(43):37555–37565

41. Ibrahim SS, Ayesh AS (2015) Electrical and optical properties of functionalized multiwalled carbon nanotubes/poly (3-octylthiophene)/polystyrene composites. J Thermoplast Compos Mater 28(2):225–240

42. Che BD, Nguyen BQ, Nguyen L-TT, Nguyen HT, Nguyen VQ, Le TV, Nguyen NH (2015) The impact of different multi-walled carbon nanotubes on the X-band microwave absorption of their epoxy nanocomposites. Chem Cent J 9:10

43. Elimat ZM, Zihlif AM, Ragosta G (2010) Optical characterization of poly (ethylene oxide)/alumina composites. Physica B Condens Matter 405:3756–3760

44. Abu El-Fadl A, Soltan AS, Aashour AS, Nashaat AM (2018) Optical investigation of thermally evaporated $Cu_5Ge_xTe_{95-x}$ thin films. Mater Res Innov 22(2):69–78

45. Devangamath SS, Lobo B (2020) Optical parameters of epoxy-$CoSO_4.7H_2O$ polymer hybrid material. Mater Res Innov 24:152–160

46. Al-Mudhaffer MF, Nattiq MA, Jaber MA (2012) Linear optical properties and energy loss function of Novolac: epoxy blend film. Arch Appl Sci Res 4(4):1731–7140

47. El-Rahman MA, Yassien KM, Yassene AA (2019) Effect of gamma irradiation on the optical properties of epoxy resin thin films. Optik 183:962–970

48. Xie A, Zhang K, Sun M, Xia Y, Fan Wu (2018) Facile growth of coaxial Ag@polypyrrole nanowires for highly tunable electromagnetic waves absorption. Mater Des 154:192–202

49. Ebrahimi I, Gashti MP (2016) Chemically reduced versus photo-reduced clay–Ag–polypyrrole ternary nanocomposites: comparing thermal, optical, electrical and electromagnetic shielding properties. Mater Res Bull 83:96–107

50. Ebrahimi I, Gashti MP (2018) Polypyrrole–MWCNT–Ag composites for electromagnetic shielding: comparison between chemical deposition and UV-reduction approaches. J Phys Chem Solids 118:80–87

51. Kim K-S, Kim I-J, Park S-J (2010) Influence of Ag doped graphene on electrochemical behaviors and specific capacitance of polypyrrole-based nanocomposites. Synth Met 160(21–22):2355–2360

52. Aradhanaa R, Mohanty S, Nayak SK (2018) High performance epoxy nanocomposite adhesive: effect of nanofillers on adhesive strength, curing and degradation kinetics. Int J Adhes Adhes 84:238–249

53. Li Y, Kessler MR (2013) Liquid crystalline epoxy resin based on biphenyl mesogen: effect of magnetic field orientation during cure. Polymer 54:5741–5746

54. Lavorgna M, Romeo V, Martone A, Zarrelli M, Giordano M, Buonocore GG, Qu MZ, Fei GX, Xia HS (2013) Silanization and silica enrichment of multiwalled carbon nanotubes: synergistic effects on the thermal-mechanical properties of epoxy nanocomposites. Eur Polym J 49(2):428–438

55. AL-Hassani E (2010) Effect of UV radiation on dielectric constant and thermal conductivity in epoxy phenol blends. Eng Tech J 28:1982–1989

56. Hussein S, Abd-Elnaiem A, Nadia A, Mebed A (2020) Enhanced thermo-mechanical properties of poly(vinyl alcohol)/poly(vinyl pyrrolidone) polymer blended with nanographene. Curr Nanosci. https://doi.org/10.2174/1573413716666200310121947

57. Timoshenko S, Goodier JN (1970) Theory of elasticity. McGraw-Hill, New York

58. Łączka M, Cholewa-Kowalska K, Kulgawczyk K, Klisch M, Mozgawa W (1999) Structural examinations of gel-derived materials of the CaO–P2O5–SiO2 system. J Mol Struct 511:223–231

59. Czarnobaj K (2008) Preparation and characterization of silica xerogels as carriers for drugs. Drug Deliv 15(8):485–492

60. Sahmetlioglu ER, Mart H, Yuruk H, Surme Y (2006) Synthesis and characterization of oligosalicylaldehyde-based epoxy resins. Chem Pap 60(1):65–68

61. Du X, Yu ZZ, Dasari A, Ma J, Mo M, Meng Y, Mai YW (2008) New method to prepare graphite nano-composites. Chem Mater 20:2066–2068

62. Khare KS, Khabaz F, Khare R (2014) Effect of carbon nanotube functionalization on mechanical and thermal properties of cross-linked epoxy–carbon nanotube nanocomposites: role of strengthening the interfacial interactions. ACS Appl Mater Interfaces 6:6098–6110

63. Gojny FH, Nastalczyk J, Roslaniec Z, Schulte K (2003) Surface modified multi-walled carbon nanotubes in CNT/epoxy-composites. Chem Phys Lett 370(5–6):820–824

64. Ma P-C, Mo S-Y, Tang B-Z, Kim J-K (2010) Dispersion, interfacial interaction and re-agglomeration of functionalized carbon nanotubes in epoxy composites. Carbon 48(6):1824–1834

65. Zeng S, Shen M, Duan P, Xue Y, Wang Z (2018) Effect of silane hydrolysis on the interfacial adhesion of carbon nanotubes/glass fiber fabric-reinforced multiscale composites. Text Res J 88:379–391

66. Ketan SK, Rajesh K (2013) Effect of carbon nanotube dispersion on glass transition in cross-linked epoxy–carbon nanotube nanocomposites: role of interfacial interactions. J Phys Chem 117(24):7444–7454

67. Peterson RE, Anderson AC (1973) The kapitza thermal boundary resistance. J Low Temp Phys 11:639–665

68. Liu H, Dong M, Huang W, Gao J, Dai K, Guo J, Zheng G, Liu C, Shena C, Guo Z (2017) Lightweight conductive graphene/thermoplastic polyurethane foams with ultrahigh compressibility for piezoresistive sensing. J Mater Chem C 5:73–83

69. Labunov VA, Basaev AS, Shulitski BG, Shaman YP, Komissarov I, Prudnikava AL, Tay BK, Shakerzadeh M (2012) Growth of few-wall carbon nanotubes with narrow diameter distribution over Fe–Mo–MgO catalyst by methane/acetylene catalytic decomposition. Nanoscale Res Lett 7:102

70. Peng-Cheng M, Shan-Yin M, Ben-Zhong T, Jang-Kyo K (2010) Dispersion, interfacial interaction and re-agglomeration of functionalized carbon nanotubes in epoxy composites. Carbon 48:1824–1834

71. Ramirez S, Chan K, Hernandez R, Recinos E, Hernandez E, Salgado R, Khitun A, Garay J, Balandin A (2017) Thermal and magnetic properties of nanostructured densified ferrimagnetic composites with graphene-graphite fillers. Mater Des 118:75–80

72. Saadah M, Hernandez E, Balandin AA (2017) Thermal management of concentrated multi-junction solar cells with graphene-enhanced thermal interface materials. Appl Sci 7:589

73. Ci L, Bai J (2006) The reinforcement role of carbon nanotubes in epoxy composites with different matrix stiffness. Compos Sci Technol 66:599–603

74. Fox M (2001) Optical properties of solids. Oxford University, New York

75. Hongbing Z, Chan Z, Wenzhe C, Minquan W (2005) Characterization and nonlinear optical property of a multi-walled carbon nanotube/silica xerogel composite. Chem Phys Lett 411:373–377

76. García V, Guerrero L, Nair MTS, Nair PK (1999) Effect of thermal processing on optical and electrical properties of copper selenide thin films. Superficies y Vacío 9:213–218

77. Yakuphanoglu F, Cukurovali A, Yilmaz I (2004) Single oscillator model and determination of optical constants of some optical thin film materials. Phys B Condens Matter 353:210–216

78. Abbady G, Qasem A, Abd-Elnaiem AM (2020) Optical parameters and electronic properties for the transition of the amorphous-crystalline phase in $Ge_{20}Te_{80}$ thin films. J Alloy and Compd 842:155705. https://doi.org/10.1016/j.jallcom.2020.155705

79. Abd-Elnaiem AM, Hassan RM, Alamri HR, Assaedi HS (2020) Comparative investigation of linear and nonlinear optical properties of As-70 at.% Te thin films: influence of Ga content. J Mater Sci Mater Electron. https://doi.org/10.1007/s10854-020-03872-z

80. Koizhaiganova R, Kim H, Vasudevan T, Lee M (2009) Double-walled carbon nanotube (DWCNT)–poly (3-octylthiophene)(P3OT) composites: electrical, optical and structural, investigations. Synth Met 159:2437–2442

81. Tauc J (1974) Optical properties of amorphous semiconductors. Amorphous and liquid semiconductors. Springer, Boston, pp 159–220

82. Mott NF, Davis EA (1979) Electronic processes in non-crystalline materials. Oxford University Press, New York

83. Bishop SG, TL Reinecke, U Strom, PC Taylor and CC Klick (1977) International conference on amorphous and liquid semiconductors (7th) at Edinburgh. No. ONRL-C-13-77. Office of naval research London (England)

84. Venkatachalam S, Mangalaraj D, Narayandass SK, Kim K, Yi J (2005) Structure, optical and electrical properties of ZnSe thin films. Phys B Condens Matter 358(1–4):27–35

85. Kale RB, Lokhande CD (2005) Influence of air annealing on the structural, morphological, optical and electrical properties of chemically deposited ZnSe thin films. Appl Surf Sci 252(4):929–938

86. Venkatachalam S, Mangalaraj D, Narayandass SK (2007) Characterization of vacuum-evaporated ZnSe thin films. Phys B Condens Matter 393(1–2):47–55